The evolution of fitness during range expansions in multiple dimensions

Kotsar Yurii[1,2] | Hikaru Matsuoka[1] | Gen Tamiya[1,2]

[1] RIKEN Center for Advanced Intelligence Project, Tokyo, Japan

[2] Tohoku University Graduate School of Medicine, Sendai, Japan

Correspondence: Gen Tamiya, RIKEN Center for Advanced Intelligence Project, Tokyo, 103-0027, Japan

Email: gtamiya@med.tohoku.ac.jp

ABSTRACT

We efficiently simulate range expansions of populations, by using our set of computer programs, on a laterally connected lattice in 1D, 2D (on a strip, and on a disk) and 3D (in a cylinder, and in a sphere). We employ a model with finite genome regions, each containing infinite sites, for a population of diploid individuals. Using the programs, we generate tens of simulation replicates to analyse the temporal evolution of mean fitness of individuals on the expansion front. We explore the model over different conditions, compare normalisation methods for fitness, and explore the case of radial (sphere) and axial (cylinder) expansions in 3D, which might apply in the analysis of the behaviour of viruses/bacteria inside a host, in the prediction of expansions of marine species in ocean environments, and even in scenarios of interstellar space colonization. In 3D expansions, we find complex spatial fluctuations in deme-average fitness values, different from those in radial 2D expansions. In axial 3D (cylinder) expansions, we determine that the highest-valued deme-average fitness lies along the axis of the expansion. We also find the fluctuation patterns of fitness in 3D cylinder expansions, similar to those previously seen in radial

expansions in 2D. In radial 2D (disk) expansions, we find that the fitness of a population undergoing multiple mutations shows a smooth combination of binary segregation pictures against each of those mutations. We confirm the accumulation of deleterious mutations -- a phenomenon known as expansion load -- in all scenarios above.

1. INTRODUCTION

Most species on Earth exhibit fluctuating habitats, and understanding the range expansions of those habitats is of great importance in evolutionary biology. Their distribution, however, is nontrivial even in a spatially deterministic model of migration, since almost all organisms have multiple segregating genetic loci which accept random mutations (which, in turn, affect the fitness, and thus, the number of individuals). Due to demes on the expansion front having less genetic variation in the early generations after colonisation, while the front is moving, a mutation (neutral, deleterious or beneficial) can fix itself on the front for many generations thereafter, but also spread back into the bulk of the population. This is the principle of *gene surfing* (Klopfstein *et al.*, 2005). Through many generations, the effect of those mutations will accumulate, if the mutations are prevalently either beneficial or deleterious (Peischl *et al.*, 2013). There is evidence to show that 70% to 90% of all mutations are deleterious (Eyre-Walker and Keightley, 2007).

This lowers the value of fitness averaged over the individuals in every deme on the expansion front – simply "*mean front fitness*" hereafter – and exacerbates the difference in fitness between the core population and the expansion front. Nevertheless, if the selection is soft, mean front fitness can never fall to zero, and a population can avoid extinction (Peischl *et al.*, 2015a). In this regime, establishing the means to quantify the change in mean front fitness over the expansion front is an important goal, the results of which have various applications in the field of population ecology, especially in the wake of some range expansions caused by climate change (Bokma, 2010; Parmesan, 2006; Pateman *et al.*, 2012; Yamano *et al.*, 2011). These cases assume a one-dimensional (1D) or two-dimensional (2D) habitat, but this change in fitness could also be modelled for three dimensions (3D), which is the focus of this study. In this case, quantifying the change in mean front fitness is important in elucidating the limits of certain marine species' and RNA viruses' capabilities to spread, or could be vital information in the planning stages of human space expansion. Since the timescale of space expeditions could extend over tens of human generations, and the conditions of colonies in outer space are stringent to the human biology, precise planning and understanding of population and fitness distribution is required. More importantly, a reliable way to simulate and understand range expansions in three dimensions is required, especially for the case of an expansion along an axis and a certain radius around it to

allow for slight deviations -- in our case, the *3D cylinder* scenario. The axis represents the direction to a distant star (system), and the slight deviations account, e.g., for the placement of intermediate colonies according to local topology.

So far, an analytical approximation to the change in mean front fitness has been constructed only for 1D (Peischl *et al.*, 2013). This prior research shows that it's difficult to construct a theoretical formula for mean front fitness for the case of range expansions with logistic growth, mutation, selection and genetic drift, and so it is valuable to create a simulation program with the purpose of generating the dynamics of a range expansion, generation by generation, and to use the simulated data to quantify the change in mean front fitness.

We base this study in part on the research in Peischl *et al.* (2013). Their study includes a C++ program, which is able to generate fitness values for each deme in a one-dimensional expansion. In their publication, some simulation results for 1D and 2D have been given, however only up to 800 generations. In our study, based on the aforementioned C++ program, as well as Gilbert *et al.* (2018), we recreate the 1D simulation program, and independently develop 2D and 3D programs, in Julia. We gather data for a longer span of generations in 1D, and test and compare different methods throughout the algorithm (such as normalisation methods).

2. METHODS

2.1 Model: genome regions with infinite sites

Our model is based largely on the model in Peischl *et al.* (2013). For all dimensions, we start with a habitat of discrete laterally connected lattice of demes, and employ a model which accepts a population of monoecious diploid individuals of size N, similar to the stepping-stone model (Kimura, 1953), but where migration is only present between adjacent demes.

In this model, each diploid individual has a genome of $2L$ independently segregating regions with no epistasis. We set $L = 20$ in this study. These regions are the basic units during genetic recombination, which occurs once per generation. During genetic recombination, regions $1 \leq k \leq L$ have a 1/2 chance to swap with their pair in $L+1 \leq k \leq 2L$. Inside these genome regions, we assume the infinite-site model, so the same segregating region could have multiple mutations. A mutation has a fixed chance μ of occurring in a gamete, and upon that, a fixed chance ϕ of being deleterious. We set this value as $\phi = 0.9$, unless stated otherwise. Deleterious; beneficial mutations change the fitness of a recombining region by $1 + |s|$; $1 - |s|$ respectively. In this study, $|s|$ is a fixed value in each simulation trial, and is called the *selection coefficient*. Multiplicative fitness is assumed. In order to model mutations, we sample the number of mutations from a

Poisson distribution with mean μ, determine whether the mutation is beneficial or deleterious, then act on the fitness of the recombining region picked randomly from a uniform distribution. Since an infinite-site model is assumed inside the genome regions, the chance of further changing the allele of the same locus is infinitesimal, thus once the mutation has affected the fitness, the multiplicative factor of its selective effect always persists in the individual fitness. The evolution of each deme's population is based on the Beverton-Holt formula for discrete logistic growth:

$$N_{t+1} = RN_t \Big/ \left(1 + N_t \frac{R-1}{K}\right)$$

where N_t is the number of individuals in a deme in generation t, $R = 2$ is the proliferation rate, and K is the constant carrying capacity, set equal to 100, unless specified otherwise.

Furthermore, we sample the actual number of offspring individuals from a Poisson distribution with mean N_{t+1}. The deme itself does not have a hard limit for the number of individuals, hence due to Poisson sampling, the number of individuals in a deme can sometimes exceed K. Finally, each generation, migration is allowed and equally occurs between all adjacent demes, with a total migration rate m. In one dimension, migration rate is simply $m/2$ to move to either of two adjacent demes. In higher dimensions, migration rate is m/l, where l is the number of laterally adjacent demes. In particular, l is 2 in 1D, 4 in 2D, and 6 in 3D. We then employ an additional check for the demes at the boundaries of the habitat: we use reflecting borders, in the sense that if migration has been initiated, the individual shall always move somewhere -- in this case, away from the boundary of the habitat.

It is difficult, in principle, to calculate a clear proportion of deleterious and beneficial mutations, since accurate measurement of the effects of single mutations is possible only when they have fairly large effects on fitness (> 1%) (Eyre-Walker and Keightley, 2007). Nevertheless, different studies are in agreement that the proportion of deleterious mutations is prevalent and is between 70% and 90% (Kim *et al.,* 2017). For instance, Sanjuan *et al.* (2004) gives the proportion of lethal, deleterious, neutral and beneficial SNP mutations in an RNA virus as ~26%, ~35%, ~ 30%, ~ 9% respectively. In our model, single mutations can only have constant deleterious (s =－0.5%) or beneficial (s =＋0.5%) effects, which can be viewed as average values of all possible mutations for $-1 < s < 0$ and $0 \leqq s < \infty$ respectively, where the weights for s = －0.5% and s = ＋0.5% (multiplicative changes in fitness of 1 - 0.005, 1 + 0.005 respectively) need to be decided. We base the weights on Sanjuan *et al.* (2004), where we consider *lethal* mutations twice as detrimental as *deleterious* mutations, and add their doubled rate (~52%) to the stated rate of deleterious mutations (~35%) to get ~87%. Without neutral mutations, the proportions become: ~90% for deleterious and ~10% for beneficial mutations. For humans, we find a similar value in more recent studies: Gao *et al.* (2015) gives a 29% probability for a mutation to be lethal or cause

sterility when it's homozygous.

2.2 Simulations

We developed multiple simulation programs in Julia to recreate different scenarios of range expansions, based on the model described above.

We divide the total number of generations into a burn-in phase and an expansion phase. During burn-in, the habitat is restricted to an area much smaller than the full space. This is said to allow the population to reach mutation-selection-drift equilibrium (Peischl *et al.*, 2013). During the expansion phase, the population is allowed to migrate freely, up until the boundaries of the habitat. In all simulation trials (1D, 2D and 3D), we picked a size of the habitat that allow the population to fill the habitat up in several hundreds to thousands of generations. Next, we describe the general algorithm of the programs (Figure 1).

We start with an array of empty demes, which are themselves arrays of individuals (Figure 2). We then pick b random demes and fill them to their carrying capacity (given in Table 1) with individuals. Every individual starts out with an array of fitness values of 1 for every genome region. For all simulations in the current study, we set this parameter b to 5. Every generation, we run a cycle over all demes: we first determine the number of offspring logistically (as described above), then, for every individual in the offspring, we iterate over each individual in the current generation, in a random order, until we find the parents for the offspring individual (we call this *draw until pass* below). Specifically, from a uniform distribution, they must draw samples that pass the fitness values of their gametes. In one case below (referenced as *first pair*), we also employ a variation wherein, instead of a running a cycle, the fate of a new individual depends on the first random pair of parents to either pass or fail the check. After this, the two parents' gametes are recombined, and mutations are introduced. The offspring individual is formed, and then allowed to migrate.

The are several parameters that the simulations take as input. We summarise them in Table 1.

The simulations output:

•**the deme-average fitness matrix** per every generation, which stores the deme-average individual fitness for every deme in the habitat,

•**population matrix** per every generation, which stores deme populations.

Our main focus is to use the output for the deme-average fitness to further calculate its average over the expansion front, and then graph the temporal evolution of the resulting mean front fitness. We do this for different dimensions and configurations, and compare it to the

analytical approximation found below in 2.3. More specifically, we find the expansion front as the collection of outermost demes, counting from the borders of the habitat to one side ($x > 0$ half-plane in 2D, and $z > 0$ half-space in 3D) in axial expansions, and all sides in radial expansions. We then find the mean of deme-average fitness values over this expansion front. The population matrix was used to confirm the logistic growth of the population, and to determine the generation at which the whole habitat was filled, i.e. the end of the expansion.

2.2.1 Normalisation of fitness

It is also common to normalise the mean front fitness. The consideration of a normalisation in time appears when we include a burn-in phase. During this phase, individuals are locked in a tight environment, and in the absence of expansion mean front fitness grows at a fast pace. It is then natural to have mean front fitness start at the same value at the onset of the expansion as the value it would have had if there was no burn-in phase. Since we set our initial value of fitness in the genome to be 1, we could normalise our mean front fitness such that the value at the onset generation is 1. To this end, we divide mean front fitness in each generation after the onset by its value at the onset of the expansion. This approach seems to yield good correspondence with data (Peischl *et al.*, 2013, 2015b). We call this method "*onset mean normalisation"* in the results below.

However, this is not the only kind of normalisation applicable. A more literal definition of normalisation could also be applied, which maps the average values of fitness of each inhabited deme to the interval [0, 1] at every generation by dividing each deme-average fitness by the maximum overall inhabited demes. A similar approach is to map the values of fitnesses of each individual by dividing individual fitnesses by the maximum fitness of all surviving individuals. We have found that these approaches result in far more rapid decline in normalised mean front fitness. We included the results of dividing mean front fitness by the maximum deme-average fitness in the graphs in *Results* as "*maximum normalisation"*. Rather thanbeing a method to equate the scale of fitness values after a certain number of generations (in our case, the burn-in period) passed with the scale of fitness values obtained without that period, "maximum normalisation" is a normalisation in space, that gives a good way of quantifying the expansion load. We can also use this method to confirm that the difference in fitness between the core population and the front population grows with time in range expansions, even when the "onset mean normalisation" yields increasing fitness with time.

2.3 Analytical approximation

An analytical approximation to the temporal evolution of mean front fitness in this model was developed in Peischl *et al.* (2013). In this approximation, migration from a deme is only assumed possible after the deme has reached the carrying capacity K. This is a good approximation for low migration rates (m), at least compared to the (logarithmic) proliferation rate $r >> m$. Once at the capacity, approximately $Km/2$ individuals migrate to further demes in one general direction (out of two). This holds especially well in axial expansions. We then only concern ourselves with those $Km/2$ individuals, since those are assumed to comprise the expansion front. We employ the Wright-fisher model of evolution of allele frequencies, but split that process into growth and sampling phases (Wahl and Gerrish, 2001). This allows us to model $T \approx \log(2m^{-1})/r$ intermediate generations of the growth phase, during which the front population undergoes only reproduction and selection against the mutation that had just occurred. This is equivalent to a model of repeated bottlenecks, and is also similar to a series of consequent founder effects.

2.3.1 Probability of fixation

We derive a more general formula for the probability of fixation in this analytical model. In Peischl *et al.* (2013),the mutant frequency x' in the next generation is given by

$$x' = \frac{x\exp[(r+s)T]}{x\exp[(r+s)T] + (1-x)\exp(rT)} = \frac{x\exp(sT)}{x\exp(sT) + 1 - x},$$

where x is the mutant frequency in the current generation. We would like to use the difference $\Delta x = x' - x$, its mean $M[\Delta x]$ and its variance $V[\Delta x]$, to find the probability of fixation of a mutation with effect s on the expansion front. We have

$$M_{\Delta x} = x' - x, \quad V_{\Delta x} = \frac{1}{2K\frac{m}{2}} x'(1-x').$$

Meanwhile, the general formula for the gene frequency distribution under irreversible mutation (Kimura, 1964):

$$u(p) = \int_0^p G(x)dx \,/\, \int_0^1 G(x)dx\,.,$$

$$G(x) = \exp\left(-\int \frac{2M_{\Delta x}}{V_{\Delta x}} dx\right).$$

In our case:

$$-\frac{2M_{\Delta x}}{V_{\Delta x}} = -2Km \cdot \frac{x - x'}{x'(1 - x')} = 2Km(e^{-sT} - 1)[(e^{sT} - 1)x + 1].$$

We do not assume small s here, and so this does not simplify further into the formula in Peischl *et al.* (2013). Next, we rearrange and define A and B:

$$-\frac{2M_{\Delta x}}{V_{\Delta x}} = 2Km(e^{-sT} - 1)[(e^{sT} - 1)x + 1] =$$

$$-\underbrace{\frac{2Km}{e^{sT}}(e^{sT} - 1)}_{A}\left[\underbrace{(e^{sT} - 1)}_{B}x + 1\right].$$

Then,

$$G(x) = e^{\frac{-AB}{2}x^2 - Ax + C}.$$

Then the integrals in Eq. 1 can be seen as Gaussian integrals. Note that $A > 0$, $B > 0$, $AB > 0$, but the coefficient of x^2 in the exponent is a minus, so we are dealing with the imaginary error function erf(x). We have:

$$\int_0^p e^{-\frac{AB}{2}x^2 - Ax + C}dx = \sqrt{\frac{\pi}{2AB}}e^{C + \frac{A}{2B}}\left[\mathrm{erf}\left(A^*(Bp + 1)\right) - \mathrm{erf}(A^*)\right],$$

$$A^* = \sqrt{\frac{A}{2B}} = \sqrt{\frac{Km}{e^{sT}}}.$$

Solving the lower integral in a similar manner, Eq. 1 becomes:

$$u(p) = \frac{\mathrm{erf}[A^*(Bp + 1)] - \mathrm{erf}(A^*)}{\mathrm{erf}[A^*(B + 1)] - \mathrm{erf}(A^*)}.$$

We have tested this function for the fixation probability in a flexible range of parameters s, m, r, K. Compared to the formula in Peischl *et al.* (2013), it gives slightly lower values of mean front fitness over time for small s and other parameters close to values used in this paper, with relative difference $\delta(\overline{w}) \sim 0.7\%$ after 1000 generations. Unfortunately, this analytical model is known to underestimate actual mean front fitness, so the difference does not contributeto the accuracy of approximation of the actual mean front fitness. On the other hand, it differs from the formula in Peischl *et al.* (2013) quite drastically, when $s \gtrsim 0.03, K \lesssim 10$. Hereafter and in the results, we employ this formula.

3. RESULTS

3.1 1D

In one dimension, we have carried out 4 trials: one long simulation over 70 replicates, which is our main trial, designed to measure the long-term behaviour of fitness in range expansions (**1**), one trial concerning the critical value of the rate of deleterious mutations (**2**), and two trials employing a different approach to generating the offspring in the model (**3**, **4**). All trials are roughly one-directional, in the sense that individuals start in the leftmost demes of the habitat, and we measure the front as the (moving) populated outermost demes on the right.

1) We ran 70 simulation replicates, each with a burn-in phase and active phase of 10000 and 2500 generations respectively; as well as 70 replicates without the burn-in phase. Figure 3 shows the evolution of mean front fitness in time over 70 simulation replicates. Along with it, we have also run the program from Peischl *et al.* (2013) to simulate 10 and 20 replicates of the expansion with identical parameters (all of the parameters are given in Table 1). The rise after approximately 1930 generations of free expansion corresponds to the generation in which the population filled up the whole habitat, thus raising fitness due to efficient selection. For simulations with the burn-in phase was present, we also display the results of applying different normalisation methods ("onset mean normalisation" and "maximum normalisation" in Figure 3).

2) We have also performed a trial of the formula for the critical value of the rate of deleterious mutations, below which an expansion with the parameters used in **1** (and given in Table 1) would always have increasing mean fitness at the front (Peischl *et al.*, 2013). We calculated this value to be equal to $\phi_c \sim 0.57$. Setting the parameter of $\phi = 0.45$, and running a simulation for 700 burn-in generations and 300 generations after the onset of the expansion, we successfully confirmed that our program gives an increasing trend of normalised mean front fitness during a range expansion, evenwith 10 simulation replicates (Figure 4). It can be assumed that an identical trial, ran over several tens of replicates, would yield, on average, increasing normalised mean front fitness for any value fairly close to $\phi_c \sim 0.57$.

3) In another trial, we have employed the "first pair" approach that we have described in Chapter 2.1, and likewise ran 50 simulation replicates with and without the burn-in phase, with the same parameters as in **1**. The resulting mean front fitnesses (both normalised with the "onset mean normalisation" method, and no-burn-in) were within $\delta(\overline{w}) \sim 1.5\%$ of both the results in **1** with the same normalisation, for the span of 2500 generations.

4) Continuing the analysis of the "first pair" approach, we ran two parallel trials under more extreme conditions. The results are shown in Figure 5. We can see that, similar to the result in **3**,

for mean front fitness with applied "onset mean normalisation", the trend in both approaches is identical, and the difference in values is within several percent, excluding the rough fluctuations near the onset of the expansion (presumably due to a small sample of simulations).

3.2 2D strip

In two dimensions, we likewise focused on developing simulation programs capable of confirming the results of prior research, concerning the evolution of mean fitness on the expansion front, as well as simulating and visualising the evolution of average fitness at every deme. Specifically, we developed two programs in 2D: expansion on a strip, and expansion on a disk. Below we talk about the main trial we carried out with the former program.

We created a program to simulate a range expansion roughly along an axis in two dimensions. We call this "2D strip" expansion, due to the habitat constituting a long rectangle, and give the parameters in Table 1. Individuals start in the leftmost demes of the habitat, and we measure the front as the (moving) populated outermost demes on the right. We ran 10 simulation replicates, each with a burn-in phase and an active phase of 1000 generations both; and the same number of replicates without the burn-in phase. Figure 6 (top) shows the evolution of mean front fitness in time, averaged over 10 simulation replicates. We have also displayed the non-normalised mean front fitness for reference. Furthermore, we have displayed the results of applying different normalisation methods.

In addition, we have generated animations of a heatmap that shows the evolution of deme-average fitness throughout the whole expansion at every point in the habitat. Specifically, we generated heatmaps for deme-average fitness and normalised deme-average fitness. In this case, normalisation is such that the average fitness $\overline{w_{x,y}}(t)$ at each deme (x, y are space coordinates, t counts generations from the onset of the expansion; negative t is allowed in the presence of a burn-in phase) is divided by $\overline{\overline{W}}(0)$, the average fitness over the whole habitat at the onset of the expansion. These animations can be found in the Colab repository (see "Supporting information"). A snapshot of the heatmap of deme-average fitness is given in Figure 6 (bottom).

3.3 2D disk

Next, we have simulated a range expansion on a 2D disk, which is bounded by the circle equation at a certain radius -- parameters are given in Table 1. Aside from this space boundary, the individual movement is not constrained. At the start, the founder individuals were put in the centre of the habitat. We have performed one trial, where we likewise found the evolution of mean front fitness in time, averaged over 10 simulation replicates. This result, with different normalisation

methods, is shown in Figure 7. Similar to 2D strip, we have generated heatmaps that show the temporal evolution of (normalised) average fitness at every deme in the habitat, at every generation. This heatmap is available as an animation (see "Supporting information"). A snapshot of the heatmap of deme-average fitness is given in Figure 7 (right).

3.4 3D cylinder

The main goal of this study was to build a novel simulation program that can produce data for range expansion in three dimensions, and analyse the evolution of mean front fitness consistently with the results from 1D and 2D. In particular, we developed two programs for 3D: expansion in a cylindrical habitat, and expansion in a sphere. Here, first, we describe the trial we carried out using the former program.

In this trial, we contained a population inside of a cylinder, that is constrained by a circle equation at the lateral surface and a barrier at both ends of the cylinder. This trial was roughly one-directional, meaning that the individuals started in the lowermost demes of the z-axis, and we measured the front as the (moving) populated highest demes in the direction of the z -axis. We ran 13 simulation replicates, each with a burn-in phase and an active phase of 1000 generations both; and the same number of simulation replicates without the burn-in phase. Figure 8 (left) shows the evolution of mean front fitness in time, averaged over 13 simulation replicates. As before, we also display the non-normalised mean front fitness for reference and the results of applying different normalisation methods, in Figure 8 (left). We have also generated three-dimensional heatmaps of deme-average fitness, a snapshot of which can be seen in Figure 8 (right). The animations of these heatmaps are available in "Supporting information". A typical slice image of the heatmap at height $z = 22$ and generation 200 is presented in Figure 10 (left).

3.5 3D sphere

Finally, we developed a simulation program for an expansion bounded by a 3D sphere of a constant size. At the start, the founder individuals were put in the centre of the habitat. We have performed one trial, where we likewise found the evolution of mean front fitness front in time, averaged over 15 simulation replicates. This result, with different normalisation methods, is shown in Figure 9. Similar to other trials, we have generated heatmaps for deme-average fitness at each generation. Sample animations of these heatmaps are available in "Supporting information". A snapshot of the heatmap of deme-average fitness is given in Figure 9 (right). A typical slice image of the heatmap at height $z = 18$ and generation 642 is presented in Figure 10 (right).

4. DISCUSSION

4.1 1D

Even though we have only used 10 and 20 replicates of simulation data generated with the program provided in previous research, we can see that simulations generated with our program yield close values and behaviour (relative error of normalised mean front fitness ≤ 1% everywhere expect the first 170 generations). The discrepancy between the analytical approximation and simulatedvalues grows visibly during longer expansions.

We have confirmed that the onset mean normalisation method yields values of mean front fitness for simulations with a burn-in phase closest in value to mean front fitness for simulations without a burn-in phase. Cf. the normalisation method where all demes are mapped to the interval [0, 1] every generation ("maximum normalisation" in Figure 3). The rapidly decreasing mean front fitness normalised via "maximum normalisation" can be used to measure the growing difference between the fitness in the core population and on the expansion front.

In trials **3**,**4**, we saw that the population cannot go extinct in range expansions in idealistic settings with soft selection (cf. range shifts, Gilbert *et al.* (2018)). As expected, in severe conditions, the mean front fitness in "first pair" populations was extremely low compared to "draw until pass" populations. However, when applying the “onset mean normalisation” method, these fitness values were almost equal throughout the expansion. Hence, we can say that onset mean normalisation preserves the trend well, and mean front fitness for these two offspring generation approaches differs only in scale of the absolute value.

4.2 2D

Our 2D disk simulations show that, in an expansion where the population is free to move in 4 directions (quasi-isotropically), segregation patterns resembling spokes or circular sectors emerge practically from the start of the expansion (Figure 7). This behaviour has been observed extensively in bacterial mixtures with only a single mutant allele (Hallatschek and Nelson, 2010; Korolev *et al.*, 2010). Moreover, the behaviour was recently confirmed in originally monospecific populations partially or fully developing specialist subpopulations during the expansion (Li and Kardar, 2022). Our results show that this binary segregation behaviour (i.e. with zones where the mutant allele frequency is strictly 0 or 1) changes into a picture with smooth transitions between

predominantly mutant and predominantly non-mutant zones in expansions of populations with multiple mutation types. This is speculated to be a blend of separate binary segregation pictures against each of those mutations (no matter received before or during the expansion). This was shown in part in Excoffier et al., 2008. The simple model used in this study can be approximated by a model with co-dominant mutations for low s, and it should be noted that for dominant or recessive mutations this behaviour might be different.

On the other hand, in our 2D strip trial shown in Figure 6, large-scale spatial deviations from the monotonous decrease in fitness with distance from the core population were not present in the narrow space we have set up. We've run separate trials to confirm that this is only the case with narrow expansions that approach an axial expansion such as the 1D expansion, and is also dependent on the simulation parameters such as the selection coefficient and migration rate. Cf. other simulations with wide rectangles ($0 \leq y \leq 20$) (Peischl *et al.,* 2015b).

4.3 3D

This is the first time that range expansions of this type were simulated in 3D. The deme-average fitness in **3D cylinder** (Fig. 8, right) was found to exhibit patterns of smooth combination of binary segregation pictures, similar to the those observed in **2D disk** (Fig. 7, right), but with more variation in shape, no more resembling spokes or circular sectors. This pertains to the concurrent variation in the lateral xy plane with the variation along the z -coordinate. The joint variation the greater that the variation of these effects separately. The combination of radial and axial variations here provides a more extreme fitness distribution, where any slight deviation from the central expansion axis has a chance to result in a drastic falloff in fitness. This means that, aside from the monotonous decrease in fitness proportional to the distance from the origin, future space colonisers would need to take into account the dramatic variation in fitness when straying from the central axis.

On the other hand, the mean front fitness can still be approximated fairly well using the analytical formula for one-directional 1D expansions. This is also the case for the spherical expansion (Fig. 9). Moreover, in all of the expansion scenarios in 2D and 3D, mean front fitness could still be well approximated with the analytical formula for simple one-directional 1D expansions. We assume this follows from the fact that, for each deme at the front, the probability to colonise a further deme is approximately equal to the probability to remain in the present population. However, a thing to note is the sudden drop in mean front fitness just after the onset of the expansion in simulations with a burn-in phase. This is a flaw of the burn-in phase, and could be explained by the fact that the population at the time of the onset experiences the lifting of a migration restriction, and this allows it to migrate and undergo the biggest loss of genetic

diversity per deme, since the population is still comparatively small.

Genetic drift was shown to be a factor in heterozygosity gradients in a population (Liu *et al*., 2006), and in future studies, it would be of value to analyse the distribution of heterozygous loci and calculate the temporal change in expansion-front heterozygosity in different dimensions. To this end, a finite-site model with dominance would be required. Some of the scenarios were analysed with such a model in a previous work (Peischl *et al.*, 2015b). Upon modifying our programs to a finite (1000 and more) number of loci, the calculations turned out to be computationally intensive in multiple dimensions, requiring almost 5 times the runtime as the infinite-site, finite-region model in 3D. In future studies, it would be of interest to also develop simulations that assume hard selection. Nonetheless, the infinite-site finite-region model used in this study proved to be an efficient tool for studying the general properties of expansion load.

5. CONCLUSION

A set of programs was developed for efficiently simulating range expansions in different habitats in 1, 2 and 3 dimensions. Using them, range expansions in three dimensions were successfully simulated for the first time. Different normalisation methods were investigated. “Maximum normalisation" was found to be useful to measure the growing difference between the fitness in the core population and on the expansion front. In radial 2D (disk) expansions, deme-average fitness of a population that underwent multiple mutations was found to show a smooth combination of binary segregation pictures against each of those mutations. This pattern was also observed as a component in the deme-average fitness in 3D expansions. Overall, complex fluctuations in deme-average fitness, different from those in radial 2D expansions, were found in 3D expansions. Axial 3D (cylinder) expansions were found to have the highest fitness along the axis of the expansion.

Conflict of interest statement

The authors declare no conflicts of interest.

Supporting information

We have uploaded a portion of the programs, data used in the study, as well as some animations to: *https://github.com/Vindenatt/fitness-multiple-dims*. The program files (“*programs*”) are of two types: generation and analysis. The generation files don't have a suffix. These include programs in the Notebook form, for easy tinkering and development, and *.jl* files that were used to run on a

remote machine via multiprocessing. The data from them was used to generate files in the "*data*" folder. Program files that have the suffix "*analysis*" are programs that analyse the data generated in the generation programs, and output graphs etc. We have also uploaded animations of the heatmaps for results of 2D and 3D simulations to the "*animations*" folder.

BIBLIOGRAPHY

Klopfstein, S., Currat, M. and Excoffier, L. (2005). The fate of mutations surfing on the wave of a range expansion. Molecular Biology and Evolution, 23 (3), 482-490.

Peischl, S., Dupanloup, I., Kirkpatrick, M. and Excoffier, L. (2013). On the accumulation of deleterious mutations during range expansions. Molecular Ecology, 22 (24), 5972-5982.

Eyre-Walker, A. and Keightley, P. D. (2007). The distribution of fitness effects of new mutations. Nature Reviews Genetics, 8 (8), 610-618.

Peischl, S., Kirkpatrick, M. and Excoffier, L. (2015a). Expansion load and the evolutionary dynamics of a species range. The American Naturalist, 185 (4), E81-93.

Peischl, S. and Excoffier, L. (2015b). Expansion load: recessive mutations and the role of standing genetic variation. Mol Ecol, 24: 2084-2094.

Gilbert, K. J., Peischl, S. and Excoffier, L. (2018). Mutation load dynamics during environmentally-driven range shifts. PLOS Genetics, 14 (9), e1007450.

Bokma, F. (2010). Speciation and patterns of diversity. Syst Biol, 59: 365-367.

Parmesan, C. (2006). Ecological and evolutionary responses to recent climate change. Annual Review of Ecology Evolution and Systematics, 37: 637-669.

Pateman R. M., Hill J. K., Roy D. B., Fox R., Thomas C. D. (2012). Temperature-dependent alterations in host use drive rapid range expansion in a butterfly. Science, 336: 1028-1030.

Yamano H., Sugihara K., Nomura K. (2011). Rapid poleward range expansion of tropical reef corals in response to rising sea surface temperatures. Geophysical Research Letters, 38.

Kimura M. (1953). Stepping stone model of population, Annual Report of the National Institute of Genetics, Japan, 3, 62.

Beverton R, Holt S (1957) On the Dynamics of Exploited Fish Populations. Fisheries Investigation Series 2 (19). Ministry of Agriculture, London, Fisheries and Food.

Kim B., Huber C., Lohmueller K. (2017). Inference of the distribution of selection coefficients for new nonsynonymous mutations using large samples. Genetics. 206(1), 345–361.

Sanjuan, R., Moya, A. and Elena (2004). The distribution of fitness effects caused by single-nucleotide substitutions in an RNA virus. Proceedings of the National Academy of Sciences of the United States of America, 101 (22), 8396-8401.

Gao, Z., Waggoner, D., Stephens, M., Ober, C. and Przeworski, M. (2015). An estimate of the average number of recessive lethal mutations carried by humans. Genetics, 199 (4), 1243-1254.

Wahl, L. M. and Gerrish, P. J. (2001). The probability that beneficial mutations are lost in populations with periodic bottlenecks. Evolution, 55 (12), 2606-2610.

Kimura, M. (1964). Discussion models in population genetics. Vol. 1. : Cambridge University Press.

Gilbert, K. J., Peischl, S. and Excoffier, L. (2018). Mutation load dynamics during environmentally-driven range shifts. PLOS Genetics, 14 (9), e1007450.

Hallatschek, O. and Nelson, D. R. (2010). Life at the front of an expanding population. Evolution, 64 (1), 193–206.

Korolev, K. S., Avlund, M., Hallatschek, O. and Nelson, D. R. (2010). Genetic demixing and evolution in linear stepping stone models. Reviews of Modern Physics, 82 (2), 1691–1718.

Li, L. H. and Kardar, M. (2023). Specialization at an expanding front. Phys. Rev. E 108, L032402.

Liu H., Prugnolle F., Manica A., Balloux F. (2006) A geographically explicit genetic model of worldwide human settlement history. American Journal of Human Genetics, 79, 230–237.

Excoffier, L., & Ray, N. (2008). Surfing during population expansions promotes genetic revolutions and structuration. Trends in ecology & evolution, 23(7), 347–351. https://doi.org/10.1016/j.tree.2008.04.004

APPENDIX A. Floating point error

Due to operating memory limitations, we used Float32 arrays to store fitness values. Since the fitness of founders exponentially influences the fitness of next generations, we designed a test for cumulative errors in mean front fitness values.

We performed the test both for 1D and 3D. In 1D, we ran 15 simulation replicates with the default parameters given in Table 1, however only for 1000 burn-in generations and 1000 generations after onset. These were run both by a program which employs Float32, and one which

employs Float64. For every simulation, we synchronised the random seeds given to both programs. We calculated the average over 15 replicates of the mean front population and mean front fitness for each generation, for outputs of both of the programs. We then analysed the relative difference between the averages in the two programs. The difference in average population was negligible, with relative error $\sim 0.3\%$. The difference in average deme fitness was likewise unimportant with the value $< 0.3\%$.

In 3D, we ran 10 simulation replicates for both programs with the default parameters given in Table 1, but setting 100 burn-in generations and 600 generations after onset. Both differences had a maximum at the last generation in the simulation, indicating that this could be a cumulative floating-point error. The maximum of the relative difference in mean front population was $\sim 0.6\%$, while the maximum of the relative difference in mean front fitness was also $\sim 0.6\%$.

It goes without saying, that this is a comparison between Float32 and Float64, and not between Float32 and an ideal floating-point datatype. Still, this error component is was found not likely to influence the results of the tests described above in a significant way.

Parameter	1D (4)	1D (1,2,3)	2D strip	2D disk	3D cylinder	3D sphere
Burn-in generations	800	10000	1000	1000	1000	500
Generations after onset	1400	2500	1000	500	1000	150
Space size (burn-in)	$1 \leq X \leq 5$		$1 \leq X \leq 5$, $1 \leq Y \leq 10$	$0 \leq R \leq 3$	$0 \leq R \leq 10$, $1 \leq Z \leq 5$	$0 \leq R \leq 2$
Space size	$1 \leq X \leq 500$		$1 \leq X \leq 250$, $1 \leq Y \leq 10$	$0 \leq R \leq 100$	$0 \leq R \leq 10$, $1 \leq Z \leq 300$	$0 \leq R \leq 28$
Number of replicates	10	70	10	10	13	15
Selection coefficient	0.03	0.005				
Mutation rate	0.1	0.05				
Migration rate	0.05					
Carrying capacity	100					
Filled demes at start	5					
Proliferation rate	2					
Number of gene regions	20					

TABLE 1. List of simulation parameters and their values used in this paper.

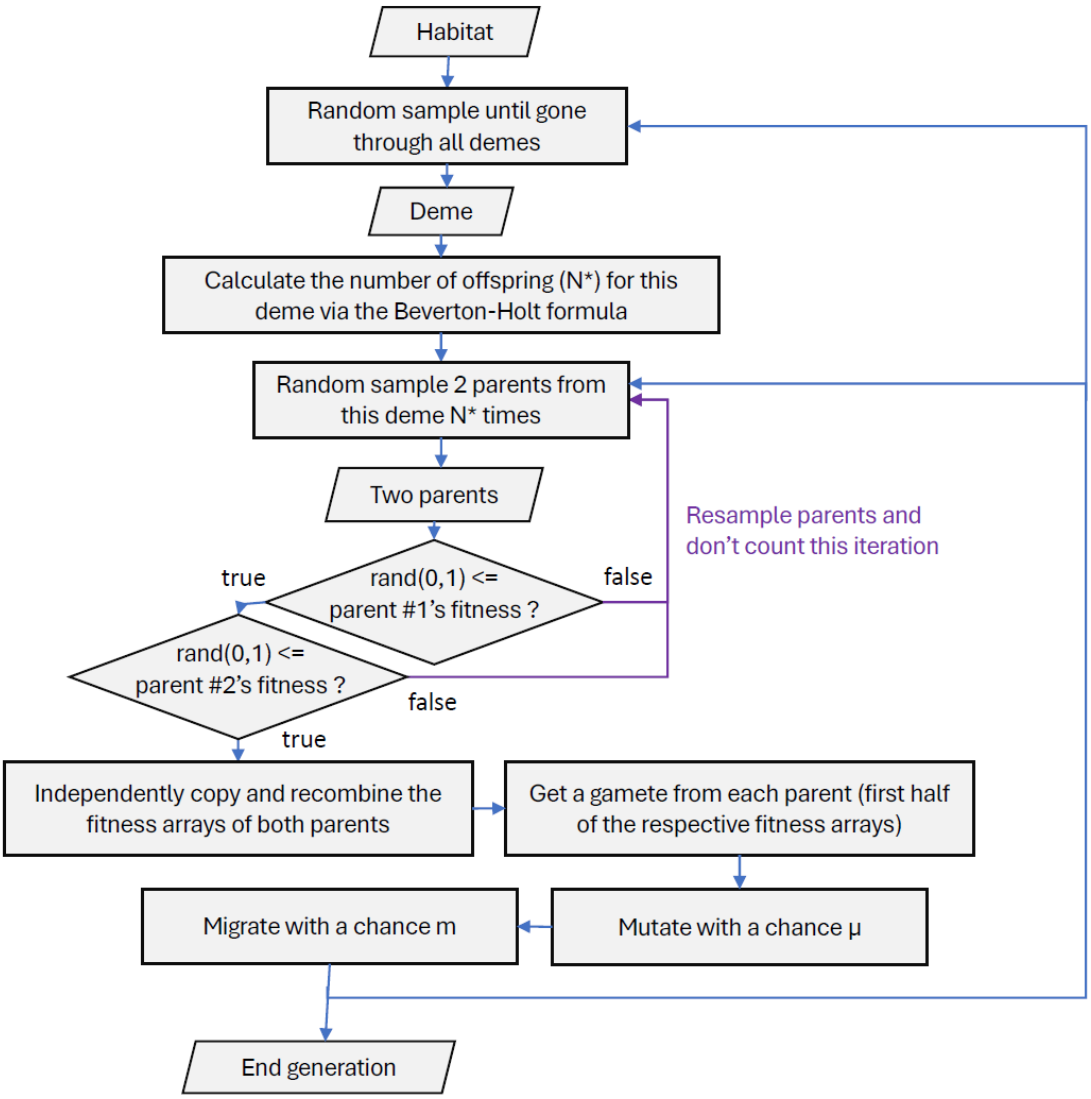

FIGURE 1. The algorithm of the cycle in each generation of expansion in our program.

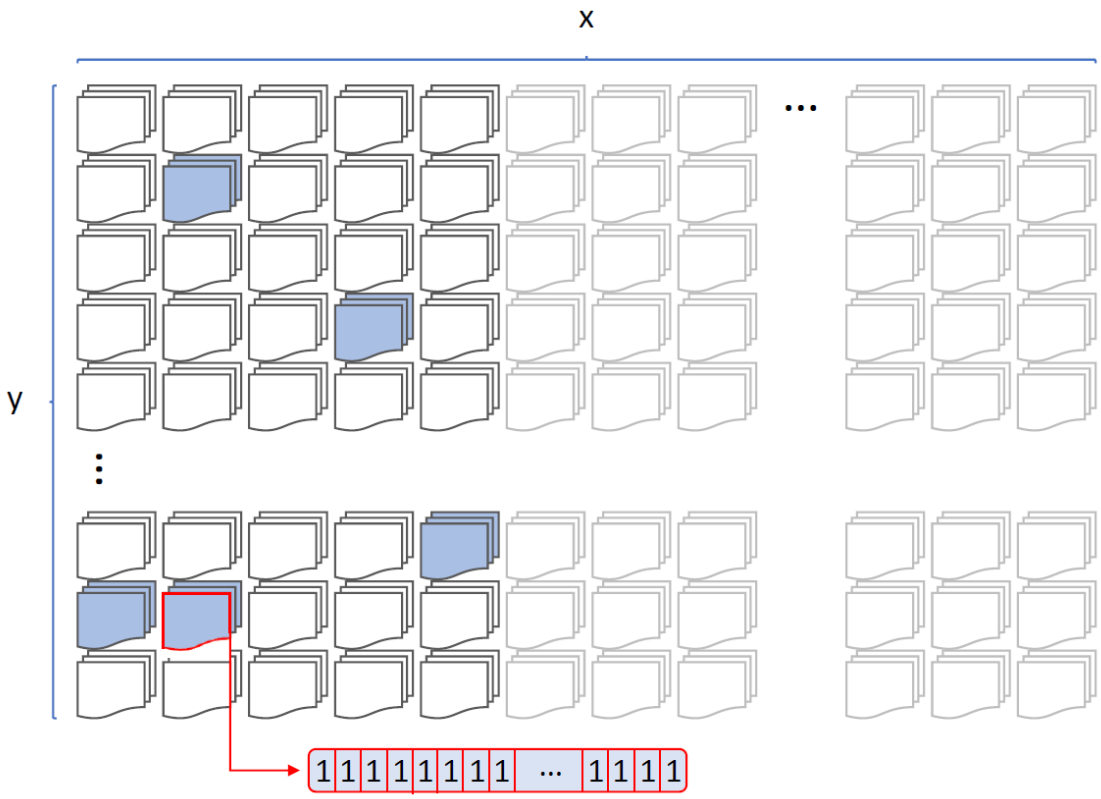

FIGURE 2. The habitat and its arrays of individuals, in the example of a 2D simulation. The x and y axes represent habitat dimensions and are given in Table 1 for specific simulations. Demes start out empty, except for *b* random demes highlighted in blue. Such demes house 100 individuals: as an example, one is highlighted in red. Their fitness values are all set to 1 at start. The faded out grey arrays/demes are unreachable during the burn-in phase.

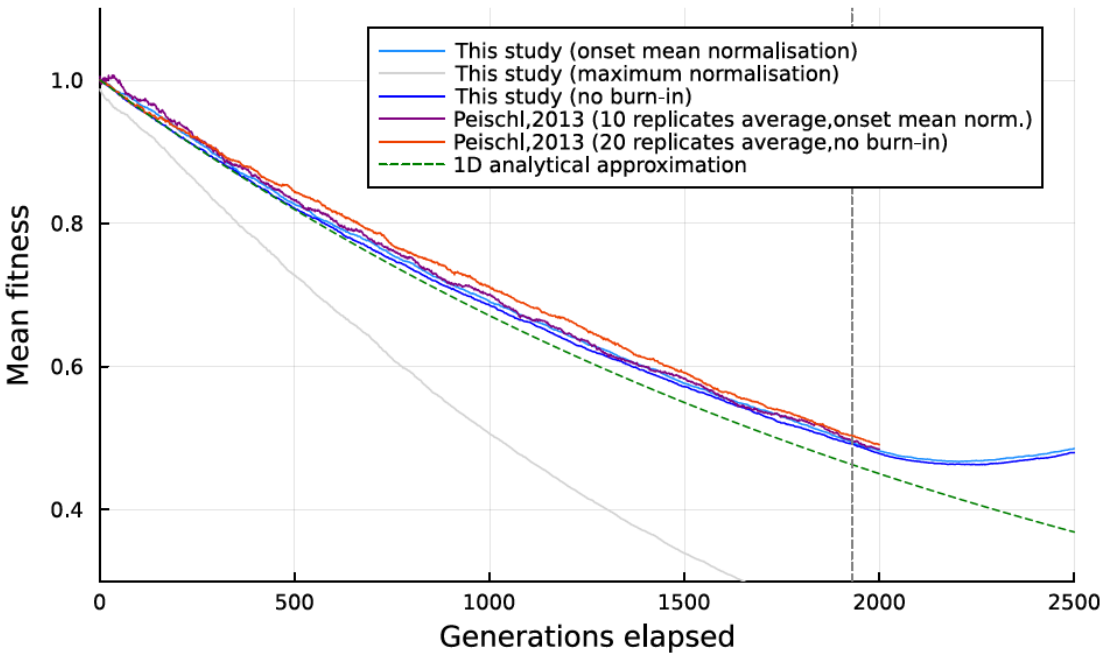

FIGURE 3. Temporal evolution of mean front fitness, as described in **1D 1**. The grey vertical line signifies the generation when all demes in the space have been filled.

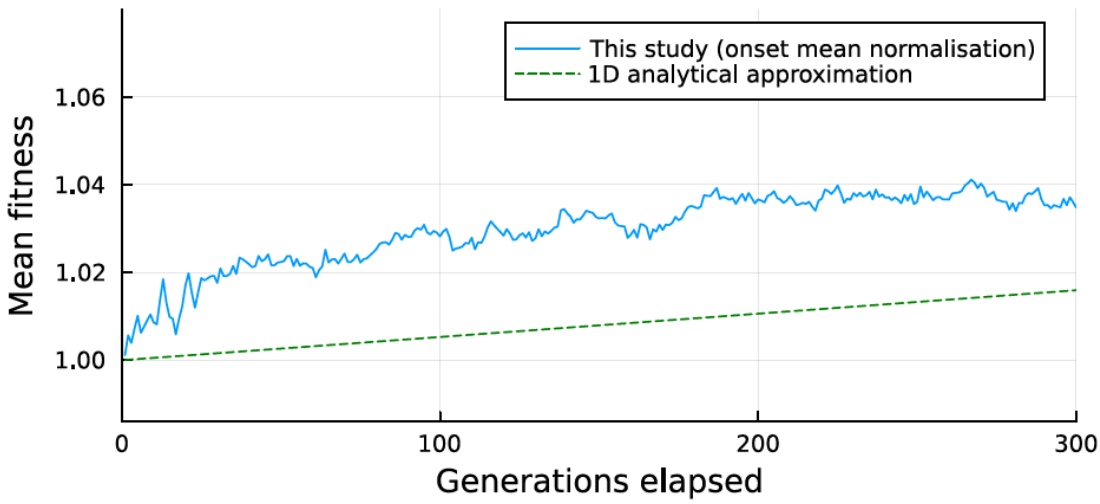

FIGURE 4. Temporal evolution of mean front fitness of a trial described in **1D 2**.

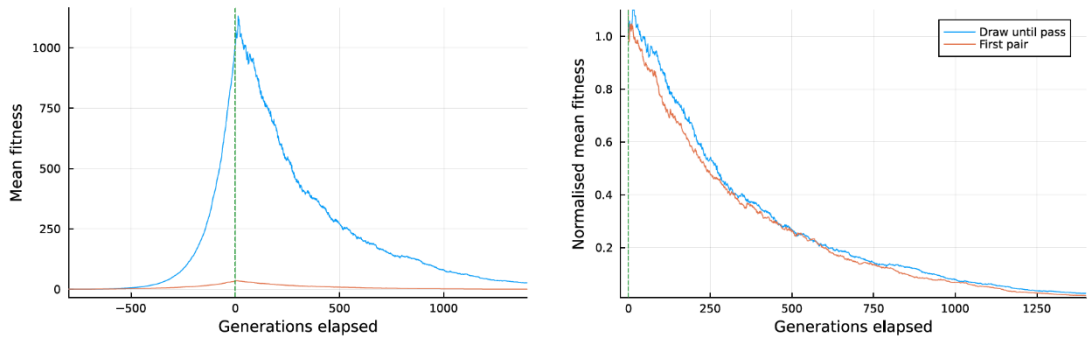

FIGURE 5. Left: temporal evolution of mean front fitness as described in **1D 4**. The green vertical line signifies the onset of the expansion; generations to the left of it constitute the burn-in phase. Right: the main expansion phase zoomed in, and mean front fitness further normalised according to the "onset mean normalisation" method.

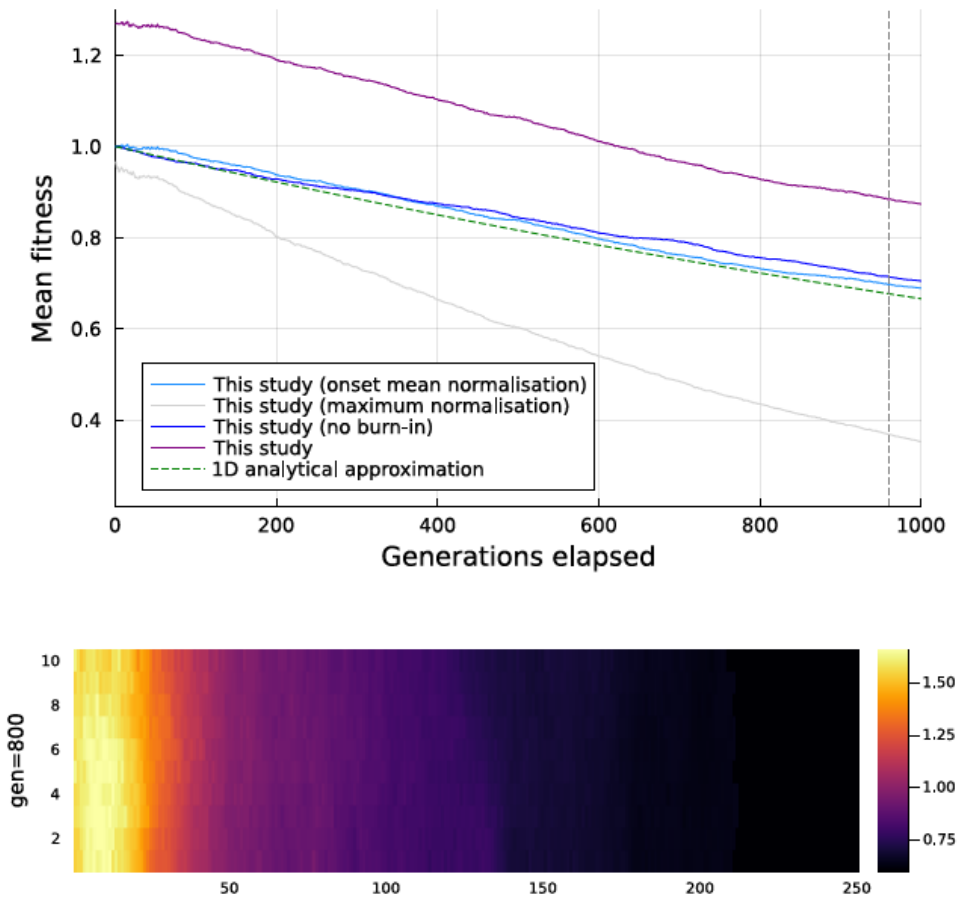

FIGURE 6. Top: temporal evolution of mean front fitness, as described in **2D strip**. The grey

vertical line signifies the generation when all demes in the space have been filled. Bottom: a snapshot of the evolution of mean deme fitness (given by the colour) at every deme in this expansion, at generation 800.

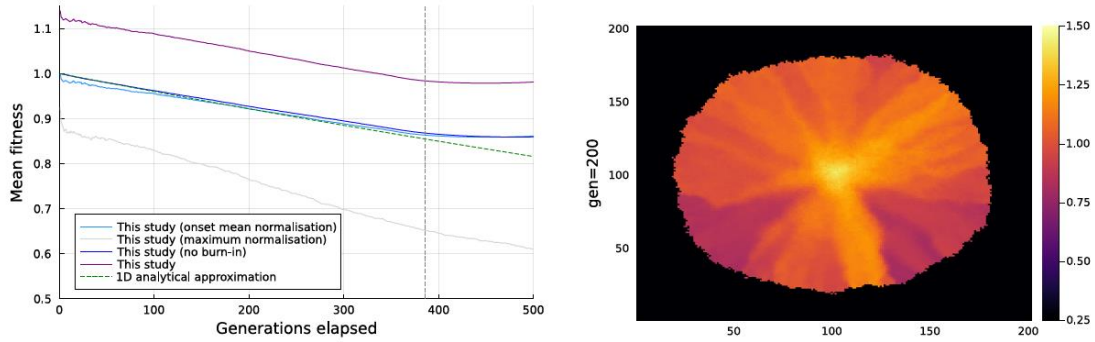

FIGURE 7. Left: temporal evolution of mean front fitness, as described in **2D disk**. The grey vertical line signifies the generation when all demes in the space have been filled. Right: a snapshot of the evolution of deme-average fitness (given by the colour) at every deme in this expansion, at generation 200.

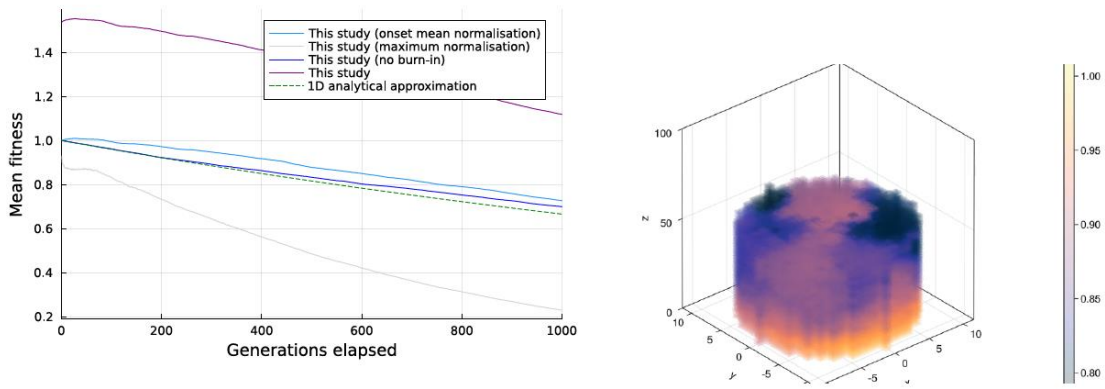

FIGURE 8. Left: temporal evolution of mean front fitness, as described in **3D cylinder**. Right: a snapshot of the evolution of deme-average fitness (given by the colour) at every deme in this expansion, at generation 46.

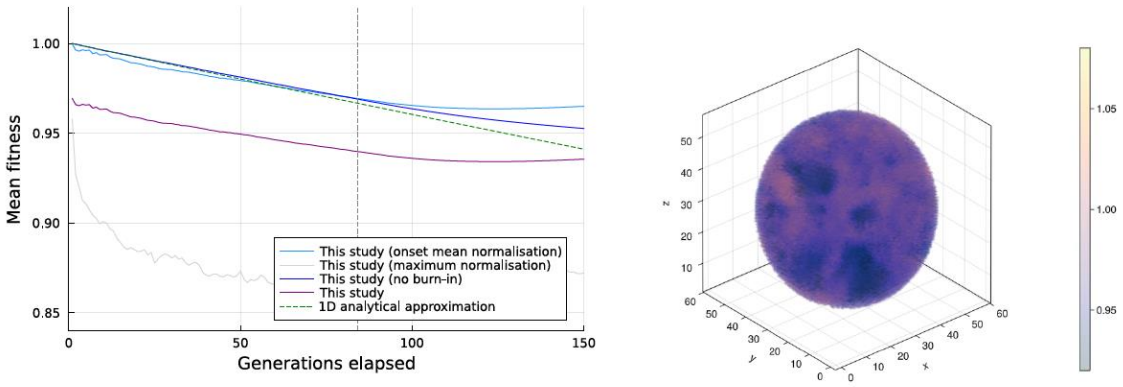

FIGURE 9. Left: temporal evolution of mean front fitness, as described in **3D sphere**. The grey vertical line signifies the generation when all demes in the space have been filled. Right: a snapshot of the evolution of mean deme fitness (given by the colour) at every deme in this expansion, at generation 75.

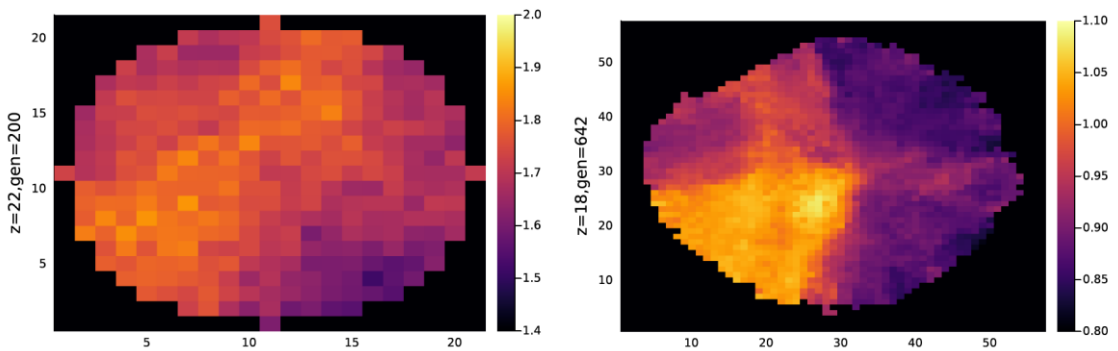

FIGURE 10. Left: a cross-section at height $z = 22$, at generation 200 after the onset of an expansion described in **3D cylinder**. Right: a cross-section at height $z = 18$, at generation 642 after the onset of an expansion described in **3D sphere**. In both graphs, the heatmap values show deme-average fitness.